

# CODED PIXELS

## *Random Coding of Pixel Shape for Super-resolution*

Tomoki Sasao<sup>1</sup>, Shinsaku Hiura<sup>2</sup> and Kosuke Sato<sup>1</sup>

<sup>1</sup>Graduate School of Engineering Science, Osaka University  
1-3 Machikaneyama-cho, Toyonaka, Osaka, 560-8531, Japan

<sup>2</sup>Graduate School of Information Sciences, Hiroshima City University  
3-4-1 Ozuka-Higashi, Asa-Minami-Ku, Hiroshima, 731-3194, Japan

Keywords: Super-resolution, Image Sensor, Richardson-Lucy Deconvolution.

Abstract: In this paper, we propose a technique to improve the performance of super-resolution by changing the effective shape of each pixel on the image sensor. Since the sampling of the incoming light by the usual image sensors is not impulse-shaped but rectangular, the high spatial frequency component of the latent image is lost through the integration effect of the pixel area. Therefore, by spraying black powder onto the image sensor we give each pixel shape a random code, which jointly aggregates the latent information of the observed scene. Experimental results show that the proposed random code greatly improves the quality of the reconstructed image.

## 1 INTRODUCTION

In recent years, multi-frame super-resolution techniques have been intensively studied to acquire a high-resolution image from a sequence of images. However, the resolution of the output image is limited even if we can use an infinite number of low-resolution input images (Tanaka and Okutomi, 2005). This limitation stems from the integration effect of each pixel shape, which determines the PSF (point spread function), and then, the image blurred by the PSF is observed by many samples. The shape of the pixel should therefore, be designed to retain the latent information of the scene. We thus propose the concept of random coding of the pixel shape to improve the performance of super-resolution. In the spatial frequency domain, a random pixel shape has no evident weak point of low response. Moreover, the random coding is suitable for various camera motions.

Since it is not easy to fabricate custom image sensors with random pixel shapes, we use black powder spread on the image sensor. The arrangement of the particles of powder is impossible to control, and thus we also propose a fast technique to determine the sensitivity distribution of each pixel using a high resolution LCD display. In this paper, we first describe the implementation of the sensor sprinkled with black powder using the method to determine the arrange-

ment of each particle, and then we present our experimental results.

## 2 RELATED WORK

One of the most relevant studies is Penrose Pixels proposed by Ben-Ezra et al. (Ben-Ezra et al., 2007). The authors argued that their Penrose tiling pattern is better for super-resolution than a square tiling because the pattern is perfectly aperiodic. However, the arrangement of the pixel position is not essential for the performance of multi-frame super-resolution since we have denser samples with an infinite number of randomly translated images. However, the shape of the pixel does affect the performance of super-resolution, because the integration of the incoming light by each pixel acts as a low-pass filter for the latent image. In other words, we observe the sampled values of the blurred image by pixel integration, and the number of input images directly corresponds to the density of the sampling. From this point of view, Penrose tiling is not optimal because it has only ten pixel shape variations including rotation.

Tanaka et al. (Tanaka and Okutomi, 2005) also discussed the problem of the theoretical limit of super-resolution due to the pixel shape if we could use an infinite number of input images. In their paper,

they pointed out that a square pixel has zero response for some spatial frequencies as shown in Figure 1. On the other hand, a Gaussian PSF is not suitable for a high magnification ratio because it loses the high spatial frequency components. From their conclusions, it is evident that the PSF of the pixel shape should retain the high spatial frequency components without zero response. However, since their theory assumes a space-invariant PSF, the potential for a space-varying PSF with assorted pixel shapes has not been investigated.

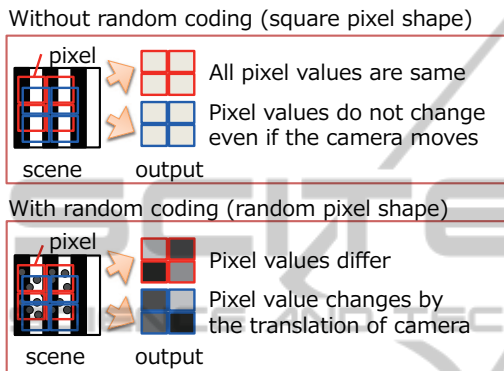


Figure 1: Advantages of random pixel shapes. If we capture a striped pattern with pitch equal to the width of each pixel, the information of the pattern is never discovered by the sensor. Contrarily, if we use a randomly coded pixel shape, the values from the pixels differ. Moreover, the change in values during the translation of the camera gives more information to recover the detail of the scene.

Of course, type of algorithm for super-resolution (SR) also matters to the quality of the reconstructed image. In general, SR algorithms can be classified into single-frame and multi-frame SR. Since the former one is obviously ill-posed, some sort of prior knowledge about the latent image is necessary. Additionally, even for the latter case, the use of priors is also very effective to obtain low-noise and sharp results. In mathematics, the reconstruction of latent image which well satisfies the statistical model of prior is classified to MAP (Maximum A Posteriori) estimation, and algorithms to find the solution have been very well investigated (Hardie et al., 1997). In addition, since pixel values in any images are always non-negative, a simple iterative algorithm called NMF (Non-negative Matrix Factorization) has been proposed (Lee and Seung, 2001). In this paper, we never discuss about pros and cons of such algorithms. In experiments, we simply applied MAP, NMF and modified version of RL (Richardson, 1972) algorithms for the reconstruction of latent images.

### 3 CODED PIXELS

In this section we introduce the idea of improving the quality of a high-resolution image reconstructed from multiple low-resolution images. As shown in Figure 1, a square-shaped pixel on the usual image sensor loses information of the input signal at a certain spatial frequency. In other words, the output of the pixel has a zero value for a signal of which the period is the same as the width of the integration, and it is impossible to reconstruct the information of the frequency. Note that all the pixels of the usual image sensor have the same shape of light sensitivity, and the lost frequency is common to all the pixels. On the other hand, a coded pixel is essentially broadband for each pixel frequency, and moreover, a different code for each pixel suppresses the ill-conditioned case by using multiple input images.

For a more specific discussion, let us consider the three types of codes shown in Figure 2. As described above, the square pixel (a) loses some of the information of the latent image. Contrarily, the impulse-shaped light sensitive pattern (b) is theoretically ideal because the spatial frequency of the impulse is broadband. However, this pattern is susceptible to a variety of noise in the actual system because the transmission of the incoming light is very small. Fortunately, the frequency response of the random code (c) varies for each pattern, and in some cases it could have zero response at a certain frequency. However, such ill-conditioned frequency is not common to the other pixels, and more input images may offer better results.

Another advantage of the random pattern is the independence from the motion of the image. If the camera motion is pure horizontal translation, both the square pixel (Figure 2(a)) and the impulse sampling (Figure 2(b)) offer no super-resolution effect for the vertical axis. On the other hand, the random pattern has no ill-conditioned case for image motion, and even the vertical spatial frequency benefits from the rewards through the horizontal motion of the scene.

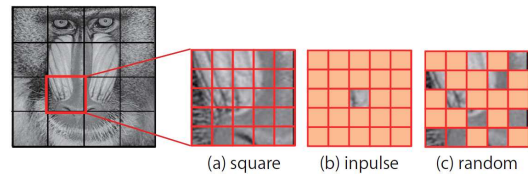


Figure 2: Differences in information provided by the code.

We can validate the effect of the random pixel shape through simulation, and in fact these results are shown later. However, since it is not easy to fabricate image sensors with arbitrary pixel shapes, we sprinkle fine black powder onto the image sensor to encode a

random pixel shape. This method raises some problems. In fact, current image sensors have so many pixels that it is not easy to find black powder with particles sufficiently smaller than the pixel size. Moreover, the arrangement and shape of the particles must be determined, because the arrangement of the particles is impossible to control. We describe a method to estimate the effective sensitivity distribution of each pixel in the next section.

### 3.1 Random Coding by Sprinkling Black Powder

Random coding is applied by sprinkling fine black powder on an image sensor. However, since the pixel size of current image sensors is so small, it is not easy to find suitable powder for sprinkling. In fact, the pixel size of the camera we used (Lumenera company, Lu125) is  $6.7 \mu\text{m} * 6.7 \mu\text{m}$ . The powder used for the coding is black toner for laser printers. Using a microscope, we determined the diameter of each particle to be about  $6 \mu\text{m}$ . Therefore, we combined several pixel values to form a large virtual pixel in the experiments. Figure 3 shows the toner on the image sensor as observed with a microscope.

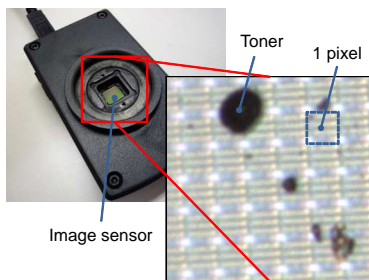


Figure 3: Toner on the image sensor.

### 3.2 Identification of Random Codes

One approach for identifying the arrangement of the particles of black powder is directly observing the image sensor using a microscope, as shown in Figure 3. However, registering the pixel positions is difficult because the contrast of the pixels on the image sensor is very low. Moreover, the arrangement of black toner does not always correspond to the distribution of the light sensitivity of each pixel. Therefore, we identified the sensitivity distribution of each pixel using the captured image of the sensor itself with controlled scene images. The principle of the identification is as follows.

- (1) Place a very small point light source in the scene, and then take an image with the contaminated im-

age sensor. The intensity values of the pixels corresponding to the position of the light source will increase, if the point light is not blocked by particles.

- (2) Repeat capturing images with a slight translation of the point light source.
- (3) The distribution of the light sensitivity of each pixel according to the position of the light source is identified.

Obviously, the resolution of the distribution of light sensitivity depends on the pitch of the translation of the point light source. This means that a more accurate identification will take longer to capture so many images when using a single light source, and thus we use a technique to shorten the measurement time by using multiple light sources. Actually, for the identification, we use an LCD display as an array of point light sources. As shown in Figure 4, the display is placed in front of the camera.



Figure 4: Relation of camera and display.

As described above, we can use multiple light sources to shorten the measurement time. In this case, it is necessary to distinguish which light source affects each pixel. In other words, each pixel should receive light from only one particular light source. Therefore, the space between two neighboring light sources should be greater than the width of light sensitivity of each pixel as shown in Figure 5. The correspondence between a pixel of the camera and the display is determined using the Gray-code measurement method. The process to determine the light sensitivity of each pixel is given below.

- (1) Vertical and horizontal stripes of Gray-code are displayed on the LCD panel, and captured by the image sensor. In the process, each pixel is associated with coordinates on the LCD panel.
- (2) The periodic dot pattern depicted in Figure 5 is displayed on the LCD panel, and an image is captured.
- (3) One lighting pixel on the LCD panel is determined by selecting the nearest lighting pixel to the coordinates corresponding to the camera pixel.

- (4) The sensitivity from the point light source to the camera pixel is recorded.
- (5) The dot pattern is shifted pixel by pixel, and then steps (2) to (4) are repeated.

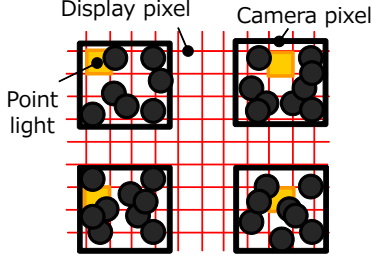


Figure 5: Projection of the dot pattern.

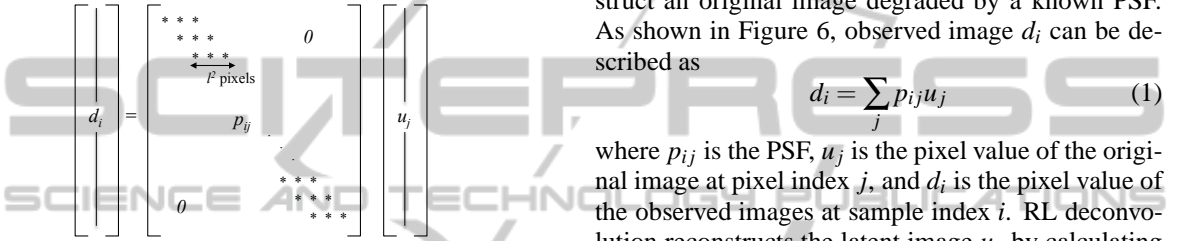


Figure 6: Sparse matrix representation of light sensitivity distribution.

Finally, we obtain the light sensitivity distribution of each pixel. The distribution obtained by this process is represented as shown in Figure 6. In the figure, vector  $d_i$  denotes the pixel value of the camera, while  $u_j$  is the intensity distribution on the LCD panel. Since the resolution of the LCD panel is higher than that of the camera, the length of  $u_j$  is longer than  $c_i$ , and matrix  $p_{ij}$  describes the relationship between the LCD panel and the camera. Since the area of light sensitivity of each camera pixel is so small, matrix  $p_{ij}$  is sparse. If the area of light sensitivity of each pixel on the LCD panel is limited to  $l \times l$ , the number of non-zero entries in each row is less than  $l^2$ , as shown in Figure 6. This characteristic is very useful not only to shorten the measurement time as described above, but also to reduce the memory requirement for the light sensitivity distribution.

For the super-resolution, vector  $u_j$  corresponds to the high-resolution latent image, and  $d_i$  is the low-resolution observed image. Therefore, the resolution of the LCD panel used to identify the distribution of particles determines the resolution of the recovered high-resolution image by super-resolution.

### 3.3 Shift-varying Richardson-Lucy Deconvolution

Usually, we assume a shift-invariant PSF for super-

resolution. However, as described above, the codes given for the camera pixels are not identical to each other. Therefore, we must deal with a shift-varying PSF in the super-resolution calculation. Unfortunately, some algorithms and frameworks for deconvolution are limited to shift-invariant PSFs. For example, we cannot use Fourier-transform based deconvolution techniques such as Wiener filters.

In this section, we present a modification of the Richardson-Lucy (RL) deconvolution (Richardson, 1972). Originally, RL deconvolution was limited to shift-invariant PSFs, but a small modification allows handling the shift-varying case, which includes random codes.

The RL algorithm is an iterative method to reconstruct an original image degraded by a known PSF. As shown in Figure 6, observed image  $d_i$  can be described as

$$d_i = \sum_j p_{ij} u_j \quad (1)$$

where  $p_{ij}$  is the PSF,  $u_j$  is the pixel value of the original image at pixel index  $j$ , and  $d_i$  is the pixel value of the observed images at sample index  $i$ . RL deconvolution reconstructs the latent image  $u_j$  by calculating the recurrence equations:

$$u_j^{(t+1)} = u_j^{(t)} \sum_i \frac{d_i}{c_i} p_{ij} \quad (2)$$

$$c_i = \sum_j p_{ij} u_j^{(t)} \quad (3)$$

Unfortunately, the original RL algorithm is limited to shift-invariant PSFs, and thus we extend it to handle the shift-varying case. In the final stage of the calculation, result  $u_j^{(t)}$  should converge to the latent image  $u_j$ , so we can lead the condition

$$\frac{d_i}{c_i} = 1 \quad (4)$$

by comparing Equations 1 and 3. In this case, the recurrence Equation 2 can be simplified as

$$u_j^{(t+1)} = u_j^{(t)} \sum_i p_{ij} \quad (5)$$

at the converged state  $u_j^{(t+1)} = u_j^{(t)}$ . Therefore, it is necessary to satisfy the following equation

$$\sum_i p_{ij} = 1 \quad (6)$$

since the reconstructed image  $u_j$  cannot be changed. However, Equation 6 is not satisfied in the case of shift-varying PSFs. Therefore, we extend the recurrence equation of the RL method as

$$u_j^{(t+1)} = u_j^{(t)} \sum_i \frac{d_i}{c_i} \frac{p_{ij}}{\sum_i p_{ij}} = \frac{1}{\sum_i p_{ij}} u_j^{(t)} \sum_i \frac{d_i}{c_i} p_{ij} \quad (7)$$

to compensate the nonuniform gain of updating the image.

## 4 SIMULATION EXPERIMENTS FOR COMPARING CODES

In this section we verify the performance of random coded pixels with the RL method through simulation.

### 4.1 Simulation Conditions

The image used in the experiment is shown in Figure 7. The super-resolution factor is  $14 \times 18$ , and the resolution of the input image is very low as shown in Figure 7(b). The assumed camera motion is horizontal with vertical pixel-wise translation of the original image. Therefore, each pixel shift on the observed image is 0.07 of the pixel width and 0.055 of the pixel height. We used 252 images with different shift values, and therefore the number of observed samples and output pixels is the same.

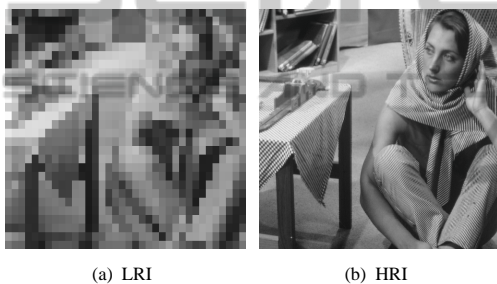


Figure 7: Original high-resolution latent image (b) and corresponding low-resolution input image (a) for the simulation experiment.

We compared the five types of codes shown in Figure 8. We divided each observed pixel into  $14 \times 18$  subpixels, and set a transmission ratio for each sub-pixel. Therefore, the size of each subpixel is the same as the latent image. Figure 8(a) simulates the usual image sensor filled with 100% square pixels. The pinhole code (b) can be considered to be an identical transform from the latent image to the input value. Codes (c) and (d) are random codes generated by different algorithms. Transmission of code (c) is a continuous value, whereas code (d) consists of randomly arranged multi-pinhole codes. Code (e) is a code for the Gaussian distribution with variance 5.0. The noise model used in the experiment is additive noise. Since smaller transmission decreases the pixel values, the worse the SN ratio becomes. For example, pinhole code (b) has 252 times larger noise relative to the signal value than the square pixels (a). We used two magnitudes of noise in the experiment. The added noise has a Gaussian distribution with zero mean and standard deviation of 1.0 and 20.0 for the 8-bit input images.

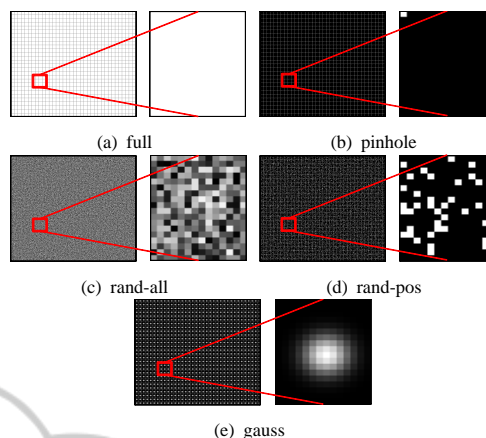


Figure 8: Codes for each pixel used in the simulation: (a) square shape of normal image sensor (aperture ratio = 100%), (b) one of  $14 \times 18$  subpixels open, very small aperture ratio (0.4%) like impulse sampling, (c) transmission ratio of all sub-pixels is random, not periodic, (d) transmission ratio of each sub-pixel is 1 or 0, randomly assigned, (e) transmission ratio has a Gaussian distribution pattern.

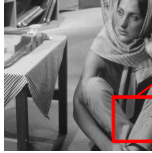
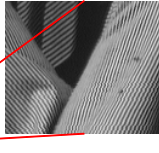
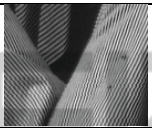
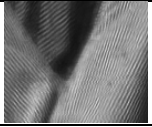
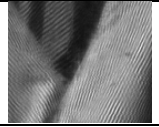
### 4.2 Results

The PSNRs of the reconstructed high-resolution images with different codes and noise values are shown in Figure 1. Magnified views of the reconstructed images are also shown in Table 1. It is clearly shown that the pinhole code (b) with little noise is the best, because the capturing process can be considered to be an identical transform. However, the result for much noise is the worst, because the sensitivity of the sensor is very low. The case of full-aperture (a) has the most light efficiency, however, the result is not at all sharp for both noise values. In the case of much noise, the rand-pos code (d) is the best in the PSNR evaluation; it is also the best in the case of little noise except for the pinhole code. The appearance of the output image using rand-pos code (d) is also the best as shown in Figure 1; in particular, the fine detail is very well reconstructed with less noise than the pinhole code.

## 5 EXPERIMENTS WITH A REAL CONTAMINATED SENSOR

We used a real camera without a cover glass and contaminated with black toner from a laser printer. First, we show the experimental results of identifying the arrangement of the particles, and then the results of super-resolution with several reconstruction algorithms.

Table 1: Super-resolution simulation results with different codings of the shape of the light sensitivity of each pixel.

barbara image		
target image		
gauss noise	little noise	much noise
full		
PSNR	22.372787	22.372758
pinhole		
PSNR	48.108994	22.180849
rand_all		
PSNR	22.515605	22.511611
rand_pos		
PSNR	25.181091	25.300695
gauss		
PSNR	23.85785	23.856232

### 5.1 Identification of Light Sensitivity Distribution

The camera used in the experiment is an Lu125 (Lumenera company) without a cover glass on the sensor. As described above, we found the average diameter of particles of the black toner to be about  $6 \mu$ . Specifications of the equipment used are given below.

- Pixel pitch:  $6.7 \mu\text{m} * 6.7 \mu\text{m}$
- Resolution of the camera: 1280\*1024
- Exposure time: 350 ms
- Resolution of LCD display: 1600\*1200

In the experiments, we used a part of the image sensor as shown in Figure 9. Here, the area of the LCD panel in the captured image is about  $360 \times 300$

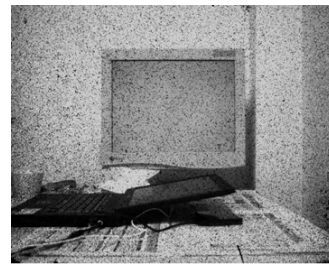


Figure 9: Arrangement of LCD panel.

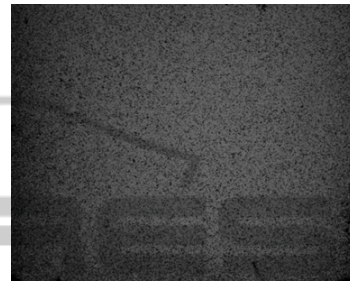


Figure 10: Input image for flat white scene.

pixels. Figure 10 shows an image of white paper taken with the coded camera. We see that the toner is scattered over the whole image sensor.

Figure 11 shows the results of the identified light sensitivity distribution of each camera pixel. Since the size of the pixel is very similar to the size of the toner particles, it is not clear whether the particle covers the pixel. Therefore, we combined  $3 \times 3$  pixel values into a single value to form larger virtual pixels, resulting in an input image size of  $120 \times 100$  pixels.

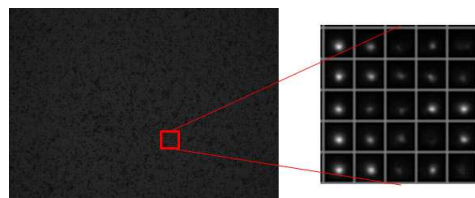


Figure 11: Estimated light sensitivity distribution of an actual pixel of the sensor with black powder.

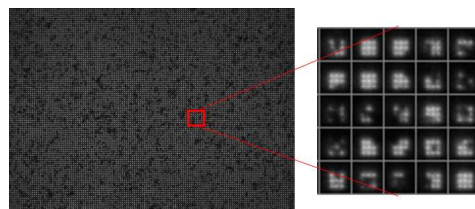


Figure 12: Estimated light sensitivity distribution of  $3 \times 3$  combined virtual pixels with black powder.

Figure 12 shows the results of the identified light sensitivity distribution of each virtual camera pixel.

Since we use  $3 \times 3$  pixels as a single pixel, the identified light sensitivity has gaps between neighboring actual gaps. Please note that we never used the raw independent pixel values, but combined only the intensity. This shows that the method for identifying light sensitivity works properly. We carried out the same process for the camera without contamination. Figure 13 shows the clear shape of the virtual pixels.

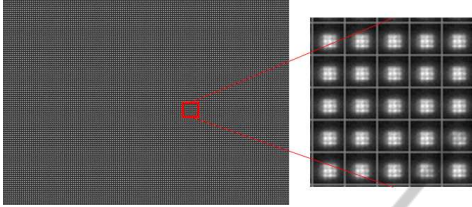


Figure 13: Estimated light sensitivity distribution of  $3 \times 3$  combined virtual pixels without black powder.

## 5.2 Super-resolution with Controlled Scene Motion

Before we attempted an experiment with unknown object motion, we carried out an experiment using images with known motion. We used the light sensitivity distribution identified in Section 5.1 (Figure 12, 13). To capture images with known motion, we used the display for calibration to show an image to the sensor. The image on the display was shifted pixel by pixel to capture images with controlled translation. The experimental conditions are as follows.

- Translation of each image is known
- Number of input images: 576
- Virtual input image: (120, 100) pixels
- Reconstructed image: (1600, 1200) pixels

The image used in the experiment is a star chart as shown in Figure 14. Figure 14(a) shows one of the input images without black powder.

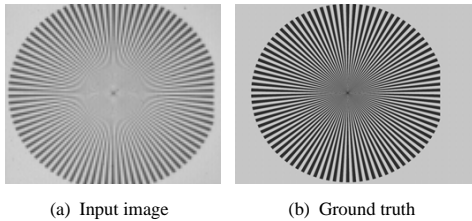


Figure 14: Image used in the experiment and captured image.

Table 2 shows the reconstructed images and quantitative evaluation result (PSNR), where INVERSE denotes the direct solution by calculating the inverse

Table 2: Super-Resolution result by coding the pixel shape.

	Chart image	
	target image	
Kind of code	@no code@	random code
INVERSE		
PSNR	11.858526	13.138333
MAP		
PSNR	9.260995	11.755036
NMF		
PSNR	11.624983	11.873994
RL		
PSNR	10.960783	12.88722

of the light transport matrix  $p_{ij}$ . MAP and NMF are the estimation with maximum-a-posteriori and non-negative matrix factorization algorithms, respectively, with a smooth edge prior. RL is the modification of the Richardson-Lucy algorithm described in Section 3.3.

The results show that the random coded sensor always produces better results for all reconstruction algorithms. In particular, the sensor without random coding shows lost spatial frequency, but the random coding suppresses such failure cases for all frequencies.

## 5.3 Experiment using Real Scene with Unknown Motion

We performed an experiment to estimate a high-resolution image from the input image shown in Figure 15. We used the light sensitivity distribution iden-

tified in Section 5.1(Figure 12,13). In this experiment, we captured 300 real images using a camera with arbitrary motion. The motion of the scene was estimated using a Phase Only Correlation (POC) algorithm (Kuglin, 1975). Since the variation in pixel sensitivity degrades the accuracy of motion estimation, we used a compensated image. More specifically, we took a picture of a flat white scene as shown in Figure 10 as a reference, and then the images of the actual scene were divided by the reference image. The compensated image looks clearer with very slight effects of contamination, so it is better for motion estimation.

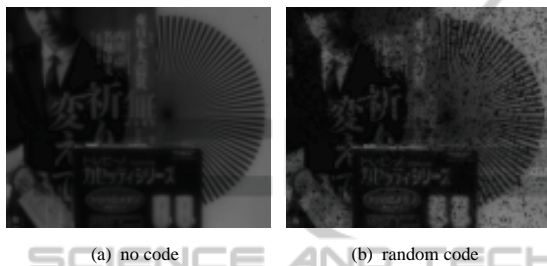


Figure 15: Observation image.

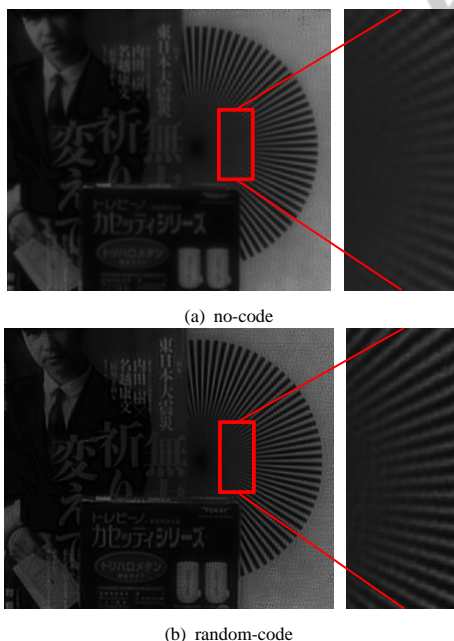


Figure 16: Super-Resolution results for no-code and random-code.

Figure 16 shows the results of applying the modified RL algorithm to the observation images for each estimated code. Although it is impossible to evaluate the result quantitatively, it is clear from the results that the randomly coded sensor is better than the one from the original sensor.

## 6 CONCLUSIONS

We focused on the loss of the high frequency component caused by the pixel shape of image sensors, and proposed a random coding for the pixel shape. In addition, we tried to implement such a device by sprinkling fine black powder on the image sensor. The arrangement of black particles was calibrated using the captured images. The results clearly show that the coded pixel has advantages for multi-frame super-resolution. We also argued that constructing a real Coded Pixel sensor is feasible with current technology. Manufacturing the image sensors with randomly shaped pixels will be a challenge in the future.

## ACKNOWLEDGEMENTS

This work was partially supported by Grant-in-Aid for Scientific Research (B:21300067) and Grant-in-Aid for Scientific Research on Innovative Areas (22135003)D.

## REFERENCES

- Ben-Ezra, M., Lin, Z., and Wilburn, B. (2007). Penrose pixels super-resolution in the detector layout domain. volume 0, pages 1–8. IEEE 11th International Conference on Computer Vision.
- Hardie, R., Barnard, K., and Armstrong, E. (1997). Joint map registration and high-resolution image estimation using a sequence of undersampled images. volume 6, pages 1621–1633. IEEE.
- Kuglin, C. (1975). The phase correlation image alignment method. In *Proc. Int. Conference Cybernetics Society*, pages 163–165.
- Lee, D. and Seung, H. (2001). Algorithms for non-negative matrix factorization. volume 13, pages 556–562. MIT Pres.
- Richardson, W. (1972). Bayesian-based iterative method of image restoration. volume 62, pages 55–59. Optical Society of America.
- Tanaka, M. and Okutomi, M. (2005). Theoretical analysis on reconstruction-based super-resolution for an arbitrary psf. volume 2, pages 947–954. IEEE Computer Society.